A Network Model for Deep Bed Filtration Processes

Equations for the deep bed filtration problem are obtained as a special case of a general model formulated earlier. The filtration coefficient λ is expressed as an explicit function of system parameters such as fluid flow rate, pore density, and pore size distribution. For a unimodal pore size distribution it is found that λ remains constant both in space and time. In general, however, λ is shown to decrease. Explicit solutions to the problem, including particle density profiles and permeability, are obtained for the two cases of large values of the coordination number Z (capillary tube model), and for a bimodal pore size distribution with a finite coordination number.

M. M. Sharma
Department of Petroleum Engineering
University of Texas
Austin, TX 78712

Y. C. Yortsos
Departments of Chemical
and Petroleum Engineering
University of Southern California
Los Angeles, CA 90089

Introduction

Mathematical models of a complex process, such as deep bed filtration, have been attempted in the past following two distinctly different approaches of increasing complexity (Tien and Payatakes, 1979): a phenomenological global approach, and a theoretical local approach. The phenomenological approach relies on postulating simple conservation and rate equations for the description of the overall behavior of deep bed filters. Starting with a particle mass balance for a linear system with constant properties

$$\phi \frac{\partial y}{\partial t} + \frac{\partial \sigma_v}{\partial t} + q \frac{\partial y}{\partial x} = 0 \tag{1}$$

the transformation

$$\tau = t - \int_0^x \frac{\phi}{q} dx \tag{2}$$

is introduced, to rearrange Eq. 1 into the form

$$\frac{\partial \sigma_v}{\partial \tau} + q \frac{\partial y}{\partial x} = 0 \tag{3}$$

In the above, y denotes particle concentration, ϕ is porosity, σ_v represents volume of particles deposited per unit pore volume, q is the superficial velocity, and x and t denote distance along the bed and time, respectively. The process of filtration is subsequently taken to be a rate process, frequently assumed to be first order with respect to concentration,

$$\frac{\partial \sigma_v}{\partial \tau} = q\lambda y \tag{4}$$

Equation 4 serves for the definition of the filtration coefficient λ, the determination of which has been the subject of numerous investigations in deep bed filtration (Ison and Ives, 1969; Ives, 1970). In general, the filtration coefficient is anticipated to depend explicitly on several system parameters and implicitly on time and the distance along the filter bed (Herzig et al., 1970; Chiang, 1983; Tien, 1983). Specific functional dependences of λ on the diameter of the filter grains (pore size) d_g, carrier fluid viscosity η_f, and fluid velocity q have been obtained by Rajagopalan and Tien (1979) and are tabulated in Table 1. The filtration coefficient was also found to vary with process time, generally decreasing with time. In certain cases, an initial short period of increasing λ has been reported and attributed to an initial increase of specific surface area. Quite frequently, however, this initial period was not observed (Tien and Payatakes, 1979). Instead, the filtration coefficient decreased monotonically as a result of a decrease in the specific surface area available for deposition and an increase in the interstitial fluid velocity.

Although convenient for experimental investigations, the phenomenological approach has definite predictive limitations. These limitations can be overcome by an alternative local theoretical approach. Using trajectory analysis, Payatakes (1973) and Rajagopalan and Tien (1976, 1979) have made significant advances toward a better understanding of the mechanisms of filtration. Trajectory analysis methods involve the numerical integration in representative unit cells of the relevant equations

Table 1. Exponent n in the Equation $\lambda \propto X^n$

Variable X	Rajagopalan (1974)	Rajagopalan (1979)	Ives (1970)	Ison & Ives (1969)	Present Study
q	-1	-1.2 to -0.2	-1	-4	$-\frac{2}{3}$
μ	-1	-1.2 to -0.2	-2	$+1.4$	$-\frac{2}{3}$
N^*	1	1	1	1	1
L	1	1	1	1	1
Pe	$-\frac{2}{3}$	$-\frac{2}{3}$	—	—	$-\frac{2}{3}$
ϕ_o	—	—	—	—	$-\frac{1}{3}$
k_o	—	—	—	—	$-\frac{1}{3}$
r_s/r_p	-2.5 to -0.2	-2 to -0.5	—	-2.4	$-\frac{2}{3}$

of motion for non-Brownian particles subject to hydrodynamic, gravitational, electrostatic, and Hamaker forces. For fixed unit cell geometry, the numerical integration leads to the determination of the local collection efficiency and the corresponding local filtration coefficient. Furthermore, the functional dependence of the rates of particle deposition on the various dimensionless parameters can be inferred numerically. This theoretical local approach provides a valuable insight into the local mechanisms for filtration processes of non-Brownian particles. However, rigorous application of the method to describe the overall global behavior of the process would require additional computations of increasing complexity.

The estimation of macroscopic quantities such as the pressure drop across the filter bed and the evolution of permeability, are currently based on Carman-Kozeny type equations. Inherent to this equation and its modifications is the assumption of a porous medium model in terms of a bundle of parallel capillaries. The resulting implication is that the permeability is uniquely determined by a single parameter, namely the porosity. The inadequacy of such models has been noted in the literature, where it was pointed out that resulting errors in pressure drop prediction are quite large (Payatakes et al., 1974). In the absence of exact results, the dependence of the pressure gradient on process parameters is alternatively expressed in terms of experimental, numerical, and empirical correlations of the form (Tien, 1983; Herzig et al., 1970)

$$\frac{(\partial p/\partial x)}{(\partial p/\partial x)_o} = F_2(\sigma; \text{system parameters}) \tag{5}$$

From the above brief literature review it is apparent that there is a lack of general consensus on the interrelation between local quantities such as the filtration coefficient, and macroscopic quantities such as pressure drop and permeability. Furthermore, considerable uncertainty exists about the evolution in time of the above variables. In this paper, we propose a simplified formulation from which the estimation of such effects can be obtained for filtration processes in porous media having a networklike structure.

Mathematical Formulation

We consider deep bed filtration processes where removal of particles from the fluid stream occurs by particle deposition on pore walls. Size exclusion effects are negligible for a properly designed filter. Following the notation of the model developed earlier (Sharma and Yortsos, 1987a) we take $r_p^* \gg r_s^*$, thus $A \gg 1$ and the integral $I_D(r_{sD}/A)$ becomes negligible for all but a negligibly small fraction of the injected particles $[I(r_{sD}/A) \ll 1]$. Similarly, the corresponding rates of pore closure due to size exclusion are negligibly small, as $r_{pD}A \gg 1$, hence $F_{sD}(r_{pD}A) = 1$.

Examination of the population balances (Sharma and Yortsos, 1987a) shows that the surviving rate terms do not explicitly involve the particle size distribution f_s; thus we may integrate the population balances over all particles sizes to obtain

$$\frac{\partial \rho_A}{\partial t} = ER\rho_s \tag{6}$$

$$\frac{\partial \rho_s}{\partial t} + \frac{\partial \rho_s}{\partial x} = -ER\rho_s \tag{7}$$

$$\frac{\partial N_p f_p}{\partial t} = CN_p\rho_s \frac{\partial}{\partial r_p}\left[f_p\left(\frac{u_R}{r_p}\right)^{1/3}\right] \tag{8}$$

where the dimensionless subscript D has been dropped for convenience. Equations 6–8 describe the local behavior of the filtration process based on the model postulates of mass-transfer limited regime and constant injection rate and porosity premises. Equations 7 and 8 consist of two nonlinear equations coupled to each other through the variable R, which is a function of N_p, f_p through u_R, and the permeability g_m. Before we proceed with the solution of the above equations, we note that in Eq. 7 the group ER represents a local dimensionless filtration coefficient. In the notation of Iwasaki (1937), Herzig et al. (1970), and Tien and Payatakes (1979) we identify

$$\lambda \propto ER = 2\pi N_p^* \left[\frac{2D^2 l_p^2 (r_p^*)^4 L^3}{q^2 k_o}\right]^{1/3} N_p \int_0^\infty (u_R r_p^2)^{1/3} f_p \, dr_p \tag{9}$$

Aside from the intricate dependence on the instantaneous pore size distribution, as yet unresolved, the functional dependence of the local filtration coefficient on other process parameters is directly apparent from Eq. 9. This dependence is, of course, exact for a filter at initial conditions. In the course of filtration, additional effects of the process parameters on the local filtration coefficient enter implicitly through the dimensionless parameter C, as will be shown later. Nevertheless, a direct comparison of the present model predictions to previously reported investigations is possible, Table 1.

We observe an exact agreement for the effects of volume density of original pores N_p^*, and local Peclet number Pe. Fair agreement exists for the effects of the flow rate q, while a discrepancy in the exponent arises for the dependence on the carrier fluid viscosity η_f. This discrepancy reflects the Levich approximation taken to represent the rate of deposition in the mass transfer limited regime. We note that in this work use is made of the Stokes-Einstein expression for the diffusivity of Brownian particles. Equations 6–9 also suggest that the local filtration coefficient is a function of time and distance along the filter bed, through the parameter C. This functional behavior is the main subject of the investigation and is elucidated for certain particular cases in the following analysis.

Method of solution

We consider Eq. 8 and observe that the dependence of N_p and f_p on x and t enters implicitly through the variable ρ_s. Specifical-

ly, by defining the new variable

$$y = \int_0^t \rho_s \, dt \tag{10}$$

Eq. 8 is transformed into an equation in terms of the variables y, r_p. Therefore, for spatially constant initial conditions, both N_p and f_p depend implicitly on distance and time through the variable y.

The method of solution is given in the supplementary material. The implicit solution obtained is,

$$y = 0 \qquad x > t \tag{11a}$$

$$x = \frac{1}{E}\int_y^{t-x} \frac{dy}{G(y)} \qquad x < t \tag{11b}$$

Finally, further substitution of this result into Eq. 7 yields the particle density profiles,

$$\rho_s = \begin{cases} 0 & x > t \quad (12a) \\ G(y)/G(t-x) & x < t \quad (12b) \end{cases}$$

where

$$G(y) = \int_0^y R(y)\, dy \tag{13}$$

We observe that given the functional dependence $G(y)$, or equivalently $R(y)$, the particle density profiles can be constructed directly.

It was previously noted that R actually represents a dimensionless form of the filtration coefficient. If, as is frequently done in the filtration literature, R is taken to be constant, Eq. 13 yields

$$G(y) = Ry \tag{14}$$

which, upon substitution into Eq. 11b, leads to the solution

$$y = (t - x)\exp(-ERx) \tag{15}$$

For this case the particle concentration profiles become

$$\rho_s = \exp(-ERx)H(t - x) \tag{16}$$

where $H(x)$ is the Heaviside step function. Equation 16 represents the familiar exponential profile, frequently employed in filtration studies with constant filtration coefficient.

The assumption of constant R, although leading to a simplified description, is inconsistent with the preceding formulation. As noted, we anticipate the filtration coefficient to vary with time and distance implicitly through the variable y. The desired functional dependence $R(y)$ is in principle obtained from the solution of the population balance for open pores, Eq. 8. In terms of the variable y, the latter reads

$$\frac{\partial N_p f_p}{\partial y} = CN_p\rho_s \frac{\partial}{\partial r_p}\left[f_p\left(\frac{u_R}{r_p}\right)^{1/3}\right] \tag{17}$$

The solution of the above equation in closed form is generally quite difficult, in view of the intricate dependence of u_R and g_m on f_p. A numerical scheme is an obvious alternative. However, in order to obtain some insight into this problem we elected to study in the remainder certain simple cases that allow an analytical treatment.

Case 1. Large Z approximation

When the coordination number Z is large, the network reduces to a model of parallel capillaries, while the effective-medium theory (EMT) becomes exact (Koplik, 1981). In this case the effective conductance g_m is explicitly related to the pore conductance distribution f_g by the expression

$$g_m = N_p \int_0^\infty g f_g \, dg \tag{18}$$

while the fluid velocity distribution becomes

$$u_R = r_p^2/8k \tag{19}$$

In view of these, Eq. 17 becomes

$$\frac{\partial(N_p f_p)}{\partial y} = CN_p\beta^{1/3}\frac{\partial}{\partial r_p}\left[f_p\left(\frac{r_p}{8g_m}\right)^{1/3}\right] \tag{20}$$

where use is made of the dimensionless relationships $k = g_m/g_{mo}$ and $\beta = g_{mo}$. The latter is the dimensionless conductance at initial conditions obtained from the solution of Eq. 18 with $N_p = 1$. We next rearrange Eq. 20 by introducing the conductance distribution f_g through the relationships

$$f_p dr_p = f_g dg \tag{21}$$

$$g = r_p^4 \tag{22}$$

and making the substitution

$$F = N_p f_g \tag{23}$$

We remark that Eq. 22 reflects the assumed cylindrical pore geometry and the resulting Poiseuille law approximation. We also note that conductances are made dimensionless on the basis of the characteristic dimensional value $g^* = \pi(r_p^*)^4/8l_p$. Upon substitution we obtain

$$\frac{\partial F}{\partial y} = \frac{2C\beta^{1/3}}{g_m^{1/3}}\frac{\partial}{\partial g}[Fg^{5/6}] \tag{24}$$

where g_m is an implicit function of y. Equation 24 is subject to initial conditions

$$N_p = 1, \quad f_g = f_{go}(g); \quad y = 0 \tag{25a}$$

thus,

$$F = f_{go}(g); \quad y = 0 \tag{25b}$$

The solution of the first-order hyperbolic partial differential equation, Eq. 24, can be obtained by the method of characteris-

tics. The procedure used is detailed in the supplementary material. The solution takes the implicit form,

$$N_p = \int_{(v/6)^6}^{\infty} f_{go}(g)\, dg \tag{26}$$

$$f_g = \frac{1}{N_p}\left(\frac{6g^{1/6} + v}{6g^{1/6}}\right)^5 f_{go}\left(\left[\frac{6g^{1/6} - v}{6}\right]^6\right) \tag{27}$$

in terms of the timelike variable

$$v = 2C\beta^{1/3} \int_0^y \frac{dy}{g_m^{1/3}} \tag{28}$$

The effective conductance g_m, thus the permeability, can be calculated directly using Eq. 18. We obtain

$$g_m = \int_{(v/6)^6}^{\infty} \left(\frac{6\eta^{1/6} - v}{6}\right)^6 f_{go}(\eta)\, d\eta \tag{29}$$

Finally, if we further denote

$$K(v) = \int_{(v/6)^6}^{\infty} \left(\frac{6\eta^{1/6} - v}{6}\right)^6 f_{go}(\eta)\, d\eta \tag{30}$$

Eq. 28 implies

$$dy = \frac{K(v)^{1/3}}{2C\beta^{1/3}}\, dv \tag{31}$$

which furnishes the connection between v and y:

$$y = \frac{1}{2C\beta^{1/3}} \int_0^v K(v)^{1/3}\, dv \tag{32}$$

Equations 26, 27, and 29 express the open pore density, the open pore conductance, hence the size distribution, and the permeability, in terms of the variable v, which is in turn related to the variable y through Eq. 32. Thus, all the above quantities, and therefore the filtration coefficient R, can be calculated explicitly as functions of the variable y. The latter is, of course, needed for the evaluation of the particle concentration profile, Eq. 12b. The computations required are minimal and involve standard routines.

The results obtained are numerically illustrated for an initial pore size distribution of the Raleigh form

$$f_p = 2r_p \exp(-r_p^2) \tag{33}$$

Plotted in Figure 1 is the evolution of the pore size distribution as a function of the variable y for filtration at constant rates. The associated permeability reduction, the increase in the pressure gradient, and the number of open pores are shown in Figure 2 for fixed values of the parameters E and C. It is evident that the largest reduction in size occurs for pores of largest radius, while smaller pores experience a significantly smaller reduction. Eventually, the size of all pores has been reduced considerably, so that after sufficiently large values of y, complete pore closure occurs. Similarly, at any fixed location the number of open pores remains almost constant for a considerably long time, and rapidly diminishes to zero as the time of pore closure is approached. By contrast, the permeability decreases smoothly. This behavior is physically interpreted by noting that by virtue of the large Z approximation, the largest radius pores are exposed to the largest portion of the flow, thus encountering and retaining the largest fraction of particles. Consequently, the rate of size reduction for such pores is the largest. On the other hand, a disproportionately smaller fraction of the flow is allocated to the smaller size pores, resulting in smaller rates of pore closure. It should be noted that this conclusion is valid only for the capillary tube model ($Z \to \infty$). For finite Z, the pore radii near the mean value will have maximum flow velocities and will close fastest, as also observed experimentally (Payatakes, 1973; Tien, 1983).

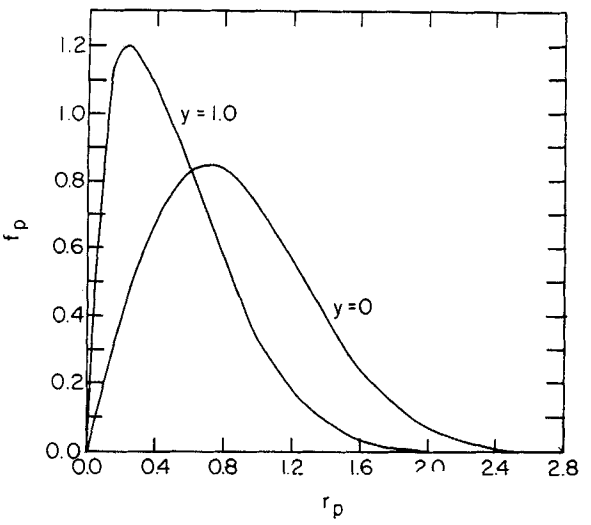

Figure 1. Evolution of pore size distribution with timelike variable y at large Z.

The filtration coefficient function $R(y)$ and the associated function $G(y)$ can be calculated directly for the particular pore size distribution by inserting Eqs. 26, 27, and 32 into Eq. 9. We note that the filtration coefficient is a monotonically decreasing function of the timelike variable y approaching zero at large values of y. The corresponding particle concentration profiles can be obtained by direct substitution into Eqs. 11 and 12. Typical

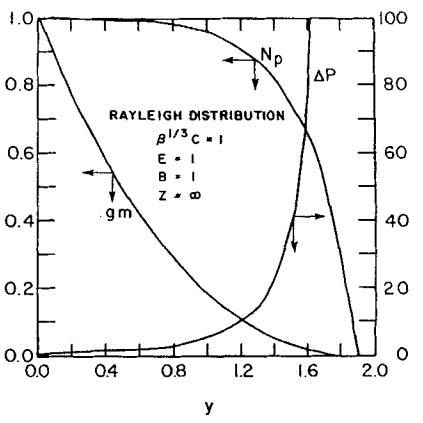

Figure 2. Evolution of number of open pores, permeability, and pressure drop with timelike variable y at large Z.

calculated concentration profiles in terms of dimensionless distance and time are shown in Figures 3 and 4. As anticipated, and contrary to the constant λ approximation, the particle concentration increases with time at any fixed location, reflecting the progressive deterioration of filtration efficiency. We note that smaller penetration of particles into the filter bed and steeper profiles result from higher values of ER_o, as expected. It is also observed that the concentration profiles, although varying with time, approximately follow an exponential distribution in distance, thereby indicating that the local filtration coefficient is approximately independent of distance in the filter bed.

A quantity of considerable interest is the gradient of the particle concentration at the inlet of the filter bed. From Eqs. 11b and 12b, the filtration coefficient at the inlet of the bed $\lambda = ER(t)$ is

$$\left.\frac{\partial \rho_s}{\partial x}\right|_{x=0} = -ER(t) \tag{34}$$

where use is made of constant concentration at $x = 0$, thus $y = t$. A plot of the filtration coefficient at $x = 0$ is shown in Figure 5. We note that the filtration coefficient decreases monotonically with time, and is a strong function of the parameter C. Higher values of C, thus of ρ_s^*, result in a more rapid decline in λ with time. We remark that a finite pore closure time is obtained. This can be calculated from Eqs. 26 and 32 by taking the limit $v \to \infty$ and recalling that $y = t$ at $x = 0$

$$t = \frac{1}{2C\beta^{1/3}} \int_0^\infty K(v)^{1/3}\, dv \tag{35}$$

In view of the properties of Eq. 30, the above integral converges. Clearly, pore closure, hence termination of filtration, is faster for larger values of C, hence larger values of injection concentration. This behavior is not predicted by constant filtration coefficient models. The present model indicates an implicit dependence of the filtration coefficient and the concentration profiles on the injected concentration. Thus, the process of deposition continuously departs during the course of filtration from a first-order rate dependence with respect to the injected concentration.

A few additional remarks are pertinent concerning the evolution of the filtration coefficient with time. As indicated in the Introduction, previous experimental investigations have reported an initial increase of the filtration coefficient for a short time followed by a continuous decrease. The initial increase, attributed to an associated enlargement of the surface area as the filter grains are coated with a monolayer of particles, is not predicted by the present model. The subsequent decrease is theorized to occur as a result of an increase in the interstitial fluid velocity and a decrease in the available area for deposition. Both of the latter phenomena are explicitly accounted for in the above analysis. Although the numerical illustrations shown pertain to the evolution in time of the filtration coefficient at $x = 0$, they represent fairly accurately the behavior of the overall coefficient as mentioned above. Furthermore, an expression for the latter can readily be derived

$$\bar{\lambda} = \frac{E \ln [G(t)/G(y)]}{1 + 1/[EG(t-1)]} \tag{36}$$

where y_1 is the value of y at $x = 1$. Although not presented here, more detailed investigations can be readily carried out using Eq. 36.

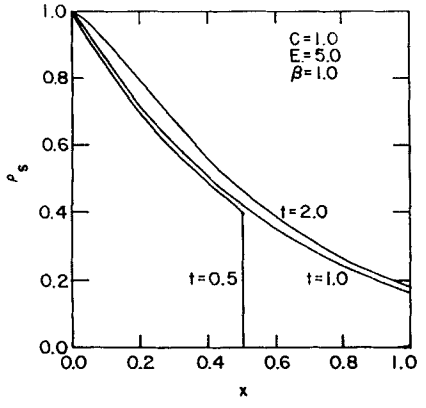

Figure 3. Particle concentration profiles at large Z.

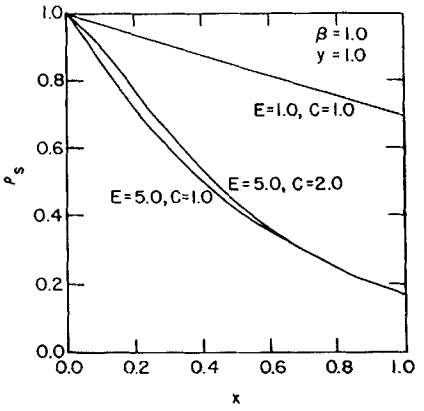

Figure 4. Particle concentration profiles for fixed time at large Z.

Case 2. Single pore size distribution

To illustrate the effect of the pore size distribution on the filtration process, we next consider filtration in a porous network

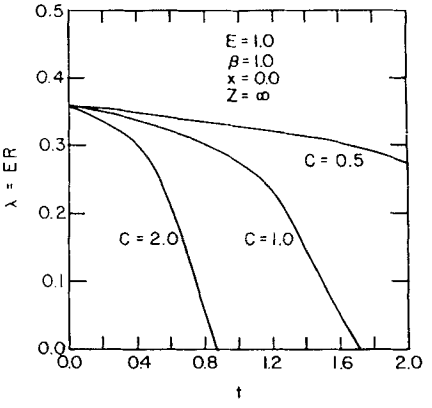

Figure 5. Evolution of filtration coefficient with time at filter inlet at large Z.

of finite coordination number Z with an initial unimodal size (conductance) distribution

$$f_{go} = \delta(g - g_{1o}) \tag{37}$$

During the course of filtration the conductance distribution remains unimodal, $f_g = \delta(g - g_1)$, while the number of open pores is constant until g_1 becomes equal to zero. For such distributions, the effective conductivity g_m is equal to g_1. To evaluate the filtration coefficient R, we use Eq. 9 to obtain

$$R = \int_0^\infty (u_R r_p^2)^{1/3} \delta(r_p - r_{p1})\, dr_p \tag{38}$$

and, in view of Eqs. A10, 34, and 35 in Sharma and Yortsos (1987a),

$$R = \beta^{1/3}/2 \tag{39}$$

Therefore,

$$\lambda = ER = N_p^* \left[\frac{2D^2 l_p^2 (r_p^*)^4 L^3 \beta}{q^2 k_o}\right]^{1/3} \tag{40}$$

We deduce that in this case the filtration coefficient remains constant and equal to its initial value throughout the process, as there is equal flow partition among the pores. The dependence of λ on the various system parameters is identical to that presented in Table 1. In contrast to the previous case, however, λ is now independent of time and the dimensionless parameter C.

For constant filtration coefficient, the concentration profiles have the exponential dependence indicated in Eq. 16. Nevertheless, the permeability continuously decreases with time as the pore sizes are reduced due to deposition. The permeability reduction is explicitly obtained for this case from Eqs. 8, 9, 21, 22, and 37. We obtain

$$\frac{\partial f_g}{\partial t} = 2C \frac{\beta^{1/3}}{g_m^{1/3}} \rho \frac{\partial}{\partial g}\left[f g^{5/6}\left(1 + \frac{g_m - g}{g + \alpha g_m}\right)^{1/3}\right] \tag{41}$$

which, in view of the fact that $f_g = \delta(g - g_m)$, yields upon substitution and rearrangement

$$g_m^{-1/2} \frac{\partial g_m}{\partial t} = -2C\beta^{1/3}\rho_s \tag{42}$$

In conjunction with the solution of Eq. 7 for constant R shown in Eq. 16, Eq. 42 admits the following solution

$$g_m^{1/2} = g_{1o}^{1/2} - C\beta^{1/3}(t - x) \exp(-ERx) H(t - x) \tag{43}$$

where R takes the value in Eq. 39. Pore closure occurs at time t_c evaluated from Eq. 43 at $x = 0$

$$t_c = g_{1o}^{1/2}/C\beta^{1/3} \tag{44}$$

Notice the functional dependence of pore closure time on the dimensionless group $C\beta^{1/3}$, lower values of C implying a larger operational life for the filter.

Case 3. Bimodal pore size distribution

As a final case, we consider a network of a finite coordination number Z with an initial bimodal pore size (conductance) distribution

$$f_{go} = (1 - p)\delta(g - g_{1o}) + p\delta(g - g_{2o}), \qquad g_{1o} < g_{2o}, \qquad 0 < p < 1 \tag{45}$$

In such processes the sizes g_1, g_2 continuously decrease and the distribution remains biomodal as long as $g_1 > 0$. For $g_1 > 0$, the number of open pores remains constant, and the effective conductivity g_m is exactly evaluated by the EMT

$$\alpha g_m^2 + p g_m[(1 + \alpha - \alpha p)g_1 + g_2(1/p - \alpha - 1)] - g_1 g_2 = 0 \tag{46}$$

where we denoted $\alpha = Z/2 - 1 > 0$. Thus, g_m can be obtained explicitly in terms of the individual conductances g_1, g_2. The latter satisfy evolution equations in time that can be derived by a procedure similar to the one used for Eqs. 24 and 41. The equations and their solution are provided in the supplementary material.

In the following numerical illustrations, the solutions are expressed in terms of the ratios

$$X = g_1/g_2 \qquad \text{and} \qquad W = g_m/g_2 \tag{47}$$

Typical profiles for the evolution of X, W, g_1, g_m, and R in terms of g_2 are shown in Figure 6 for a finite coordination number. It is generally noted that X, W, and R decrease monotonically with a decrease in g_2. The smaller pores become effectively plugged at a finite value of g_2. Beyond this point the distribution becomes unimodal and the filtration coefficient is constant thereafter. It is incidentally noted that when the fraction p is less than the percolation threshold p_c, the permeability g_m becomes identically equal to zero at the moment the smaller pores close. The sensitivity of the variables X, W, R to g_2 is significant only for small values of X_o, Figure 7. At such values the solution is quite sensi-

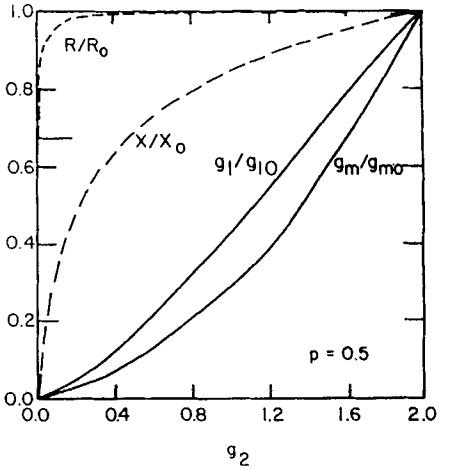

Figure 6. Variation of g_1, g_m, R, X with g_2 at $Z = 6$ ($X_o = 0.5$).

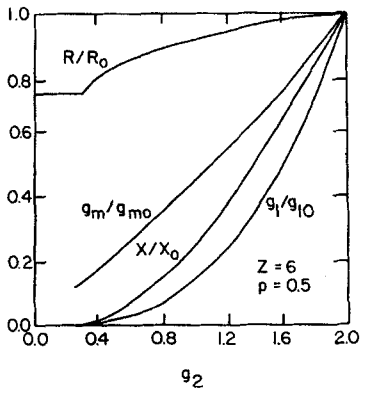

Figure 7. Variation of g_1, g_m, R, X with g_2 at $Z = 6$ ($X_o = 0.02$).

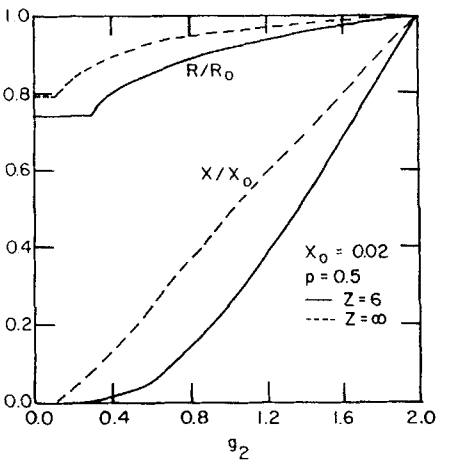

Figure 9. Variation of R and X for various z.

tive to both the coordination number, Figure 8, and the fraction p, Figure 9. Smaller values of Z and p generally lead to sharper variations in R and X, as g_2 decreases, and to a faster closure of the smaller pores.

We conclude that when X_o is not very small the two pore conductances reduce almost uniformly, the permeability remains an almost constant fraction of the largest conductance, while the filtration coefficient remains practically constant. As the closure time of the smaller pores is approached, a sharp decrease in the filtration coefficient to a lower constant value is predicted. As long as the original fraction p is larger than p_c, the ratio W, hence the permeability, also experiences a sharp decrease to a lower constant value when the closure time of the smaller pores is approached. The above behavior appears not to be very sensitive to variations in Z or p. On the other hand, a definite sensitivity is manifested when the original ratio X_o is small. For $X_o = 0.5$ the corresponding ratio in the original pore sizes is equal to 0.84, while for $X_o = 0.01$ the corresponding ratio is 0.31. Therefore, the case of small X_o is of greater significance than that for $X_o \cong 1.0$.

We next proceed to a brief discussion of the concentration profiles. The method of solution is again outlined in the supplementary material; the results are presented in Figures 10 and 11. Typical time profiles of the filtration coefficient at $x = 0$ are shown in Figure 10. As in the case of large Z, the coefficient decreases monotonically with time. The decline rates are larger for smaller Z, smaller p, and larger values of C. Note that beyond the critical time corresponding to complete plugging of pores of conductance g_1, the filtration coefficient remains constant.

The profiles are shown in Figure 11. The familiar exponential type behavior with respect to x is observed, suggesting that the filtration coefficient may not be a sensitive function of x for sufficiently large times. As shown in Figure 11, the particle concentration profiles decrease with an increase in the dimensionless parameter E. The evolution in time of the profiles follows closely the corresponding evolution in the filtration coefficient, if we recall that the slope at the origin is identical to the filtration coefficient. For instance, when X_o is not small the profiles change slowly with time until pore closure is established, while they are relatively unaffected by variations in Z or p. On the other hand, the profiles are significantly changing with time when X_o is small. As previously noted, rates of decline with time are roughly proportional to the parameter C.

Comparison with experiments

Experiments were conducted with packed beds of Ottawa sand 1 ft. (30 cm) long and 2 in. (25 mm) in diameter, into

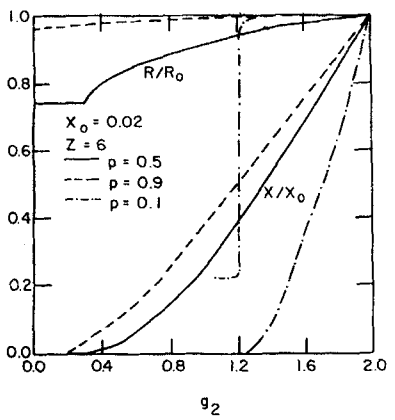

Figure 8. Time variation of R and X for various p.

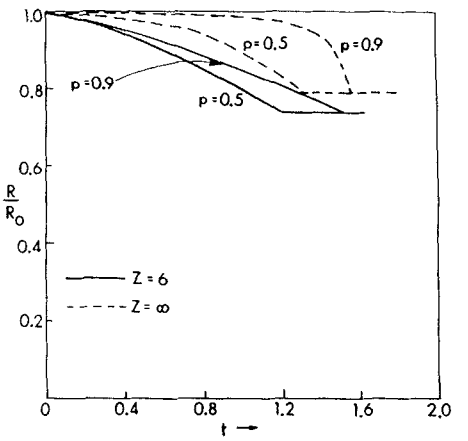

Figure 10. Filtration coefficient as a function of time.

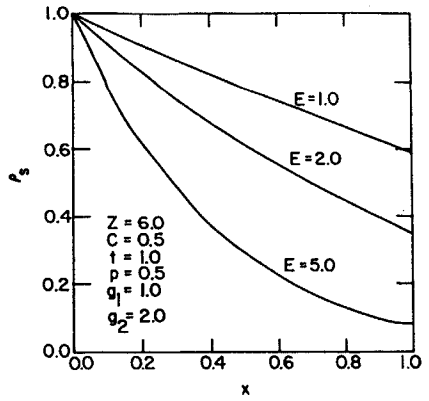

Figure 11. Particle concentration profiles at fixed time for various *E*.

which clay suspensions were injected. The pressure drop across the sandpack and the effluent particle concentration profiles were monitored for a constant flow rate. The pore size distribution of the packed bed and the particle size distributions of all injected particle streams were measured. The surface charges on the injected clay particles and the Ottawa sand were also determined. The experimental details and a complete set of results are provided elsewhere (Sharma, 1985; Baghdikian et al., 1987).

A comparison was subsequently made between the model predictions and the experimental results. First, the dependence of λ on the various system parameters as listed in Table 1 was tested, Figure 12. For small particle diameters size exclusion is negligible and the predictions of the present study agree quite well with the experimental results. For larger particles, size exclusion as well as the non-Brownian behavior of particles becomes important and the results of this study are no longer valid. The variation of the local filtration coefficient with flow rate is also adequately predicted from the persent model. The experimental results from Yao et al. (1971) are closely matched with a line of slope $-2/3$, Eq. 9.

Next, the permeability decline profiles were compared. The results for different clay injection concentrations and flow rates

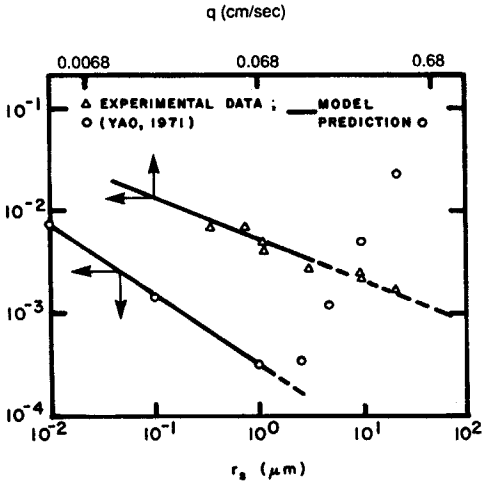

Figure 12. Variation of λ with experimentally measured quantities q and r_s.

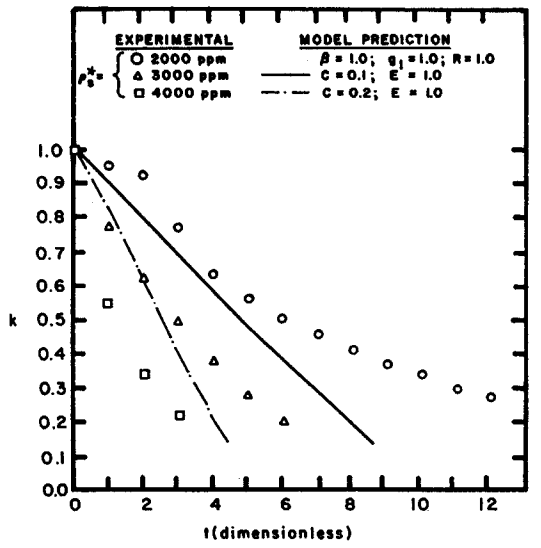

Figure 13. Permeability decline for a sandpack at various injection concentrations.

are shown in Figures 13 and 14. Since C is proportional to ρ_s^*, the results in Figure 13 show fair agreement between experiment and theory. The value of E was approximately determined from effluent and injected particle concentrations. The present model shows that changes in q affect both C and E and that large values of E and small values of C cause smaller reductions in permeability. The net effect of increases in q is to decrease both C and E. Experimental and theoretical curves for permeability reduction are shown in Figure 14. A fair agreement with experiments is noted. A partial explanation for the discrepancy at larger q may be attributed to the fact that the theoretical results plotted pertained to the large Z approximation.

Discussion

The time variation of the filtration coefficient is frequently reported to show an initial period of increasing λ. This is conjectured to occur physically because of an initial increase in the specific surface area of the filter grains. The present model does not account for any changes in surface area as particles coat the

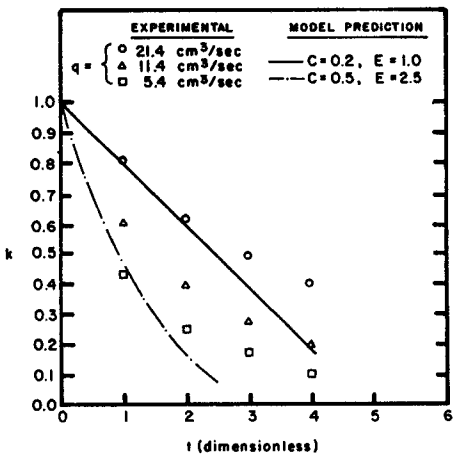

Figure 14. Permeability decline for a sandpack at various flow rates.

filter grains and hence does not predict such an initial increase. Of course, it is rather straightforward to incorporate a linear rise in specific surface area with the concentration of deposited particles until monolayer coverage, beyond which the area would remain constant and λ would decrease with time. In the declining λ region the changes in the rate of decrease with system parameters such as ρ_s^* and q are adequately described by the model.

The premises of mass-transfer control at favorable surface force interaction and absence of size exclusion effects are necessary ingredients for the application of this method. When size exclusion is important the problem becomes akin to a cake filtration or fines migration process, which is further discussed in a future publication (Sharma and Yortsos, 1987b). If kinetic control is prevailing, the local rates of deposition in Eqs. 7 and 8 take a simpler form. Following Sharma and Yortsos (1987a) one infers that, in such a case, the filtration coefficient in Eq. (7) becomes

$$R = N_p \int_0^\infty r_p f_p \, dr_p \tag{48}$$

while the population balance in Eq. 8 becomes

$$\frac{\partial N_p f_p}{\partial t} = C \rho_s N_p \frac{\partial f_p}{\partial r_p} \tag{49}$$

Equation 49 implies that the rate of decrease of a pore is independent of its size. The solution of Eqs. 48 and 49 is considerably simpler than the solutions presented above, as both equations are independent of the pore level flow distribution. The previously outlined method may then be implemented directly for the solution of this simpler problem. In this case one may work directly with the pore size distribution and subsequently obtain the effective conductivity (permeability) by making use of either the effective-medium theory or percolation theory. A preliminary analysis shows that the filtration coefficient decreases monotonically with time, the rate of decrease being independent of the coordination number. Further details can be uncovered in a straightforward fashion by directly employing the preceding analysis.

The results obtained in this paper show that the filtration coefficient is a function of time and a weak function of distance, at least for the particular cases examined. The evolution in time was found to be sensitive to the original pore size distribution and the coordination number. For pore size distributions of more complicated form than those treated above, a fully numerical solution of the population balances is of course required.

A final comment regarding the assumption of constant porosity is also pertinent. As indicated in the section pertaining to a bimodal pore size distribution, this assumption is expected to be reasonably valid as long as we recognize the existence of pore necks and pore bodies that have quite disparate sizes. It was shown that when the ratio in these sizes is of the order 1/3 or less, the size of the pore necks reduces to zero in a time interval during which the size of the pore bodies has only slightly been reduced. The corresponding change in porosity is therefore quite small. On the other hand, the model presented above can be modified to account for porosity changes for the case of dilute suspensions at constant injection rates, by removing the porosity dependence from the dimensionless time and subsequently introducing the traditional transformation shown in Eq. 2. This transformation eliminates the time derivative in Eqs. 6 and 7, while the porosity dependence of the parameter C disappears. All expressions derived above would then remain valid if the further substitution $t - x \rightarrow \tau$ is implemented.

Conclusions

The conventionally used filtration equation was shown to arise as a special case of the general population balances derived earlier (Sharma and Yortsos, 1987a). Specific methods of solution of these equations are outlined for several limiting cases. It is shown that for the model presented here the assumption of constant λ usually made in the literature is valid only for the case of a single pore size. In general, λ decreases with time and increases with distance along the filter. In addition, the functional dependence of λ on various system parameters can be determined explicitly.

The complete solution of the population balance equations is provided for three special cases. The results of these calculations show that the pore structure of the filter bed (pore size distribution and coordination number) can significantly affect filtration efficiency and permeability, and their evolution with time. The particle concentration profiles were found to be approximately exponential in distance for most cases considered. These solutions enable one to predict effluent particle concentration profiles and head losses as a function of time.

Notation

C = dimensionless parameter
D = diffusion coefficient, L^2
E = dimensionless parameter
f = size density function, dimensionless
g = pore conductance, dimensionless
k = permeability, dimensionless
l = pore length, L
L = filter bed length, L
N = number of pores per total volume, dimensionless
p = pressure, $ML^{-1} \cdot T^{-2}$
Pe = Peclet number
q = fluid superficial velocity, LT^{-1}
r_p = pore size, dimensionless
R = dimensionless parameter
t = time, dimensionless
u_R = mean fluid velocity in a pore, dimensionless
x = distance, dimensionless
y = volumetric fraction of particles, dimensionless
Z = coordination number

Greek letters

β = parameter, $=g_{mo}$, dimensionless
η = viscosity, $ML^{-1} \cdot T^{-1}$
λ = filtration coefficient, L^{-1}
ρ = concentration of particles, L^{-3}
ϕ = porosity

Subscripts

A = attached
c = critical
D = dimensionless
f = carrier fluid
m = effective
o = initial
p = pore
s = particle

Literature Cited

Baghdikian, S., M. M. Sharma, and L. L. Handy, "Flow of Clay Suspensions through Porous Media," Paper no. 16257, *Proc. 1987 SPE Oilfield Chem. Symp.*, San Antonio (1987).

Chiang, H. W., "Transient Behavior of Deep Bed Filtration," Ph.D. Diss., Syracuse (NY) Univ. (1983).

Herzig, J. P., D. M. Leclerc, and P. Legoff, "Flow of Suspensions Through Porous Media—Application to Deep Bed Filtration," *Ind. Eng. Chem.*, **62**, 8 (1970).

Ison, C. R., and K. J. Ives, "Removal Mechanisms in Deep Bed Filtration," *Chem. Eng. Sci.*, **24**, 717 (1969).

Ives, K. J., "Rapid Filtration Review Paper," *Water Res.*, **4**, 201 (1970).

Iwasaki, T., "Some Notes on Sand Filtration," *J. Am. Water Works Ass.*, **29**, 1591 (1937).

Koplik, J., "On the Effective Medium Theory of Random Linear Networks," *J. Phys. Chem. Solid State Phys.*, **14**, 4821 (1981).

Payatakes, A. C., "A New Model for Granular Porous Media: Application to Filtration Through Packed Beds," Ph.D. Diss. Syracuse (NY) Univ. (1973).

Payatakes, A. C., R. Rajagopalan, and C. Tien, "Application of Porous Media Models to the Study of Deep Bed Filtration," *Canad. J. Chem. Eng.*, **52**, 722 (1974).

Rajagopalan, R., "Stochastic Modeling and Experimental Analysis of Particle Transport in Water Filtration," Ph.D. Diss., Syracuse (NY) Univ. (1974).

Rajagopalan, R., and C. Tien, "Trajectory Analysis of Deep Bed Filtration Using Sphere-in-Cell Porous Media Model," *AIChE J.*, **22**, 523 (1976).

———, "The Theory of Deep Bed Filtration," *Progress in Filtration and Separation*, **1**, North-Holland Inc., New York, 179 (1979).

Sharma, M. M., "Transport of Particulate Suspensions in Porous Media: Applications to Filtration and Formation Damage in Sandstones," Ph.D. Diss., Univ. So. California (1985).

Sharma, M. M., and Y. C. Yortsos, "Transport of Particulate Suspensions in Porous Media: Model Formulation," *AIChE J.*, **33**(10), 1636 (Oct., 1987a).

———, "Fines Migration in Porous Media," *AIChE J.*, **33**(10), 1654 (Oct., 1987b).

Tien, C., "Deep Bed Filtration," *Handbook of Fluids in Motion*, N. P. Cheremcoff, R. Gupta, eds., Ann Arbor (MI) Science (1983).

Tien, C., and A. C. Payatakes, "Advances in Deep Bed Filtration," *AIChE J.*, **25**, 737 (1979).

Yao, K. M., ed. al., "Water and Waste Water Filtration: Concepts and Applications," *Environ. Sci. Technol.*, **5**(11), 1105 (1971).

Manuscript received June 18, 1985, and revision received May 27, 1987.

See NAPS document No. 04526 for 13 pages of supplementary material. Order from NAPS c/o Microfiche Publications, P.O. Box 3513, Grand Central Station, New York, NY 10163. Remit in advance in U.S. funds only $7.75 for photocopies or $4.00 for microfiche. Outside the U.S. and Canada, add postage of $4.50 for the first 20 pages and $1.00 for each of 10 pages of material thereafter, $1.50 for microfiche postage.